Earth and Planetary Science Letters, 45 (1979) 435-444

GEODETIC EVIDENCE FOR RIFTING IN AFAR: A BRITTLE-ELASTIC MODEL OF THE BEHAVIOUR OF THE LITHOSPHERE

A. Tarantola, Jean-Claude Ruegg, and Jean-Claude Lépine

Earth and Planetary Science Letters, 45 (1979) 435–444

[4]

GEODETIC EVIDENCE FOR RIFTING IN AFAR: A BRITTLE-ELASTIC MODEL OF THE BEHAVIOUR OF THE LITHOSPHERE

A. TARANTOLA, J.C. RUEGG and J.C. LEPINE

Laboratoire d'étude Géophysique de Structures Profondes (L.A. 195), Institut de Physique du Globe de Paris, Université P. et M. Curie, 4, place Jussieu, 75230 Paris Cedex 05 (France)

Received June 1, 1979
Revised version received July 20, 1979

An important episode of rifting occurred in November 1978 in southwest Afar, in the first subaerial section of the accreting plate boundary between the African and Arabian plates. Horizontal rifting of more than 2 m took place, with vertical displacements of about 1 m, earthquakes of magnitude up to 5.3, and a fissural volcanic eruption of basaltic lavas. Very precise geodetic measurements were carried out in order to study this crisis and strains of the order of 3×10^{-4} were measured, both tensile and compressive.

This paper presents an analysis of the mechanical behaviour of the lithosphere. It is shown that an elastic-brittle model with a rebound mechanism fits very well the data, and it is suggested that such a model, with magma injection in the resulting open fissures, should be used to describe accretion at plate boundaries.

1. Introduction

The Ghoubbat-Asal rift in the Republic of Djibouti is among all subaerial rifting zones of Afar or Iceland the most similar to a typical axial rift valley. It forms the link between oceanic parts (Gulf of Aden ridge system) and the Afar axial volcanic zones of the accreting plate boundary between the Arabian and African plates [1–4] (see Fig. 1).

Different geophysical surveys have been performed since 1971 by the Institut de Physique du Globe de Paris in this region to study the processes occurring at the plate boundaries. In particular, a high-precision geodetic network of 22 monumented points extending across a large area surrounding the rift zone was set up in collaboration with the Institut Geographique National [5].

An important seismic and volcanic crisis occurred on November 6, 1978, in this area. The major earthquakes of the crisis, with two events of magnitude larger than 5, induced an important field of normal faults and open fissures within the inner floor of the rift, and the birth of a new fissural volcano. The tectonic deformation covers an area about 3 km wide and 15 km long.

Two geodetic surveys of remeasurements were performed by means of a laser geodimeter in the few months following the crisis. Nine points surrounding the central zone were first remeasured in November 1978 just after the crisis [6]. This survey was extended in March 1979, with nine more points.

Of the 22 primitive points, one point was not found and political troubles in the region prevented us from resurveying the three northern points.

2. Experimental data

The results concerning the differences between the 1973 and 1978-79 distances, horizontally reduced to sea level, are shown in Table 1. These data have been obtained after a least squares adjustement of the geodetic net, including data of the two remeasurements.

Experimental errors have been estimated to 1 mm/

Contribution I.P.G.P. No. 335.

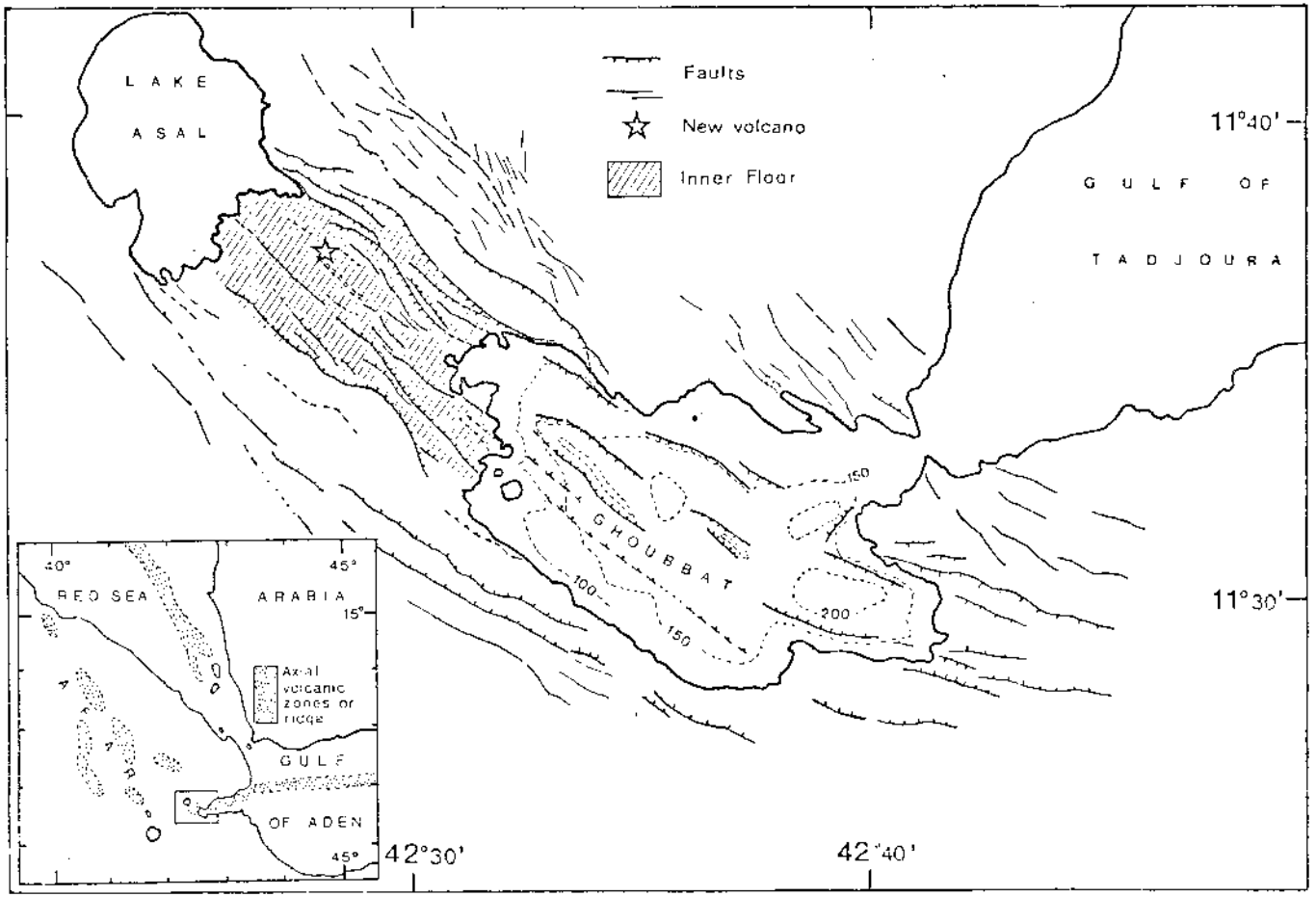

Fig. 1. Tectonic sketch map indicating the main active faults of the Asal-Ghoubbat rift zone from Stieltjes [2] and Needham et al. [4]. The lower part of the figure shows the geodynamical environment.

km. Nevetheless, some discrepancies result from small movements occurred between November 1978 and March 1979. Although these discrepancies, not exceeding a few centimeters, do not prevent us from compensating the two remeasurements together, they yield to a standard error of the distance change within about 5 cm.

These results demonstrate a large extensional deformation of the central part of the rift, reaching 2.4 m between points I and N, and a significant contraction of the two lateral margins reaching −0.7 m between points N and R (see Fig. 2 for location).

More complete description of these data will be published elsewhere [7].

3. Interpretation

The results of geodetic resurvey are often presented as displacement vectors of each station relative to an arbitrary fixed point and an arbitrary fixed direction. Such a representation allows a compact picture of the results, but it is not independent of the chosen reference frame and can lead to misinterpretation.

In order to obtain an intrinsic representation of the deformation, the region has been divided into finite triangular elements according to the geodetic net, and the mean strain tensor for each triangle has been computed. By mean strain tensor we mean the tensor that homogeneously applied to a triangle

TABLE 1

Compensated variations of distances between 1973 and 1978 for segments in Fig. 2

Segment	Distance (m)	Segment	Distance (m)
AB	0.02	HQ	0.07
AC	−0.08	HT	−0.02
AE	−0.21	IN	2.42
AF	0.29	IQ	0.12
BC	0.07	JL	- 0.05
BD	−0.23	JS	−0.01
BH	−0.04	LS	−0.01
BL	−0.18	LT	0.00
CD	−0.08	MN	−0.51
CE	−0.37	MR	0.19
DE	−0.23	NQ	1.43
DH	−0.06	NR	−0.72
DI	0.15	NU	−0.25
EF	0.96	QT	−0.20
EI	0.07	QU	0.07
EN	0.94	QV	−0.02
FM	0.04	RU	0.17
FN	−0.22	ST	0.04
HI	−0.58	TV	−0.03
HL	−0.11	UV	0.03

could exactly account for the deformation observed.

The computation has been made as follows: From the definition of the strain tensor a segment of length l is deformed by a uniform strain ϵ to a length $l + \Delta l$ given by:

$$\frac{\Delta l}{l} = \sum_{ij} \epsilon_{ij} u^i u^j \qquad (1)$$

where $\vec{u}$ is the unit vector in the direction of the segment.

For a horizontal segment:

$$\frac{\Delta l}{l} = \epsilon_{xx}(u^x)^2 + 2\epsilon_{xy} u^x u^y + \epsilon_{yy}(u^y)^2 \qquad (2)$$

Knowing the measured data $\Delta l/l$ and the values u^x and u^y for each side of a single triangle, we obtain a system of three equations in the unknowns ϵ_{xx}, ϵ_{xy} and ϵ_{yy}.

Thus, the direction and magnitude of principal horizontal strain are determined by a classical eigenvector analysis.

The results of this computation are shown in Fig. 2.

The region surrounding the axial strip shows an extensional strain roughly perpendicular to the fault directions. The two lateral edges of the rift show contraction in approximately the same direction. This is a very important point.

Tectonic observations in the inner floor of the rift valley show that brittle deformation (mostly normal faults and open fissures trending NW-SE, in the general direction of the rift) occurs inside an area not more than 3 (or 3.5) km wide in the emerged part. The assumption that this brittle deformation extends toward the Ghoubbet submarine axial structure is supported by seismic data, i.e. location of the main shock and post crisis seismicity [8].

In addition to the distance measurements, the relevelling of a line crossing the subaerial rift zone [7] shows a rough subsidence of about 70 cm strongly correlated with the tectonic observation of normal faulting.

Measured contractions in the northeast zones are larger than those in the southwest ones. This is probably due to the geometrical configuration of the network where the northwestern points are closer to the fissured region then the southern ones, and to the short wavelength of the deformation phenomenon.

The width of the brittle area is smaller than the dimensions of the central triangles. We can conclude that two opposite mechanical behaviours have occurred: an extension limited to the brittle zone, and a contraction outside. Therefore, the extension measured on the triangles in the central part should be smaller than the actual extension in the brittle zone.

Two facts can be pointed out: the coherence of the observed strain field as it is shown in Fig. 2, and the clear phenomenon of post seismic contraction, not expected a priori in a distensive rift zone.

These data suggest to us that a mechanism of elastic stretching followed by sudden breaking and elastic rebound similar to those introduced by Reid [9] for the interpretation of the 1906 San Francisco earthquake, is responsible for that phenomenon.

Thus, an elastic rebound mechanism is proposed to interpretate these data: Before a crisis, a given region in an accreting plate boundary is submitted to a tension increasing in time because of the relative drift of the plates and consequently deforms elastically. When the extensional strain reaches the elastic-

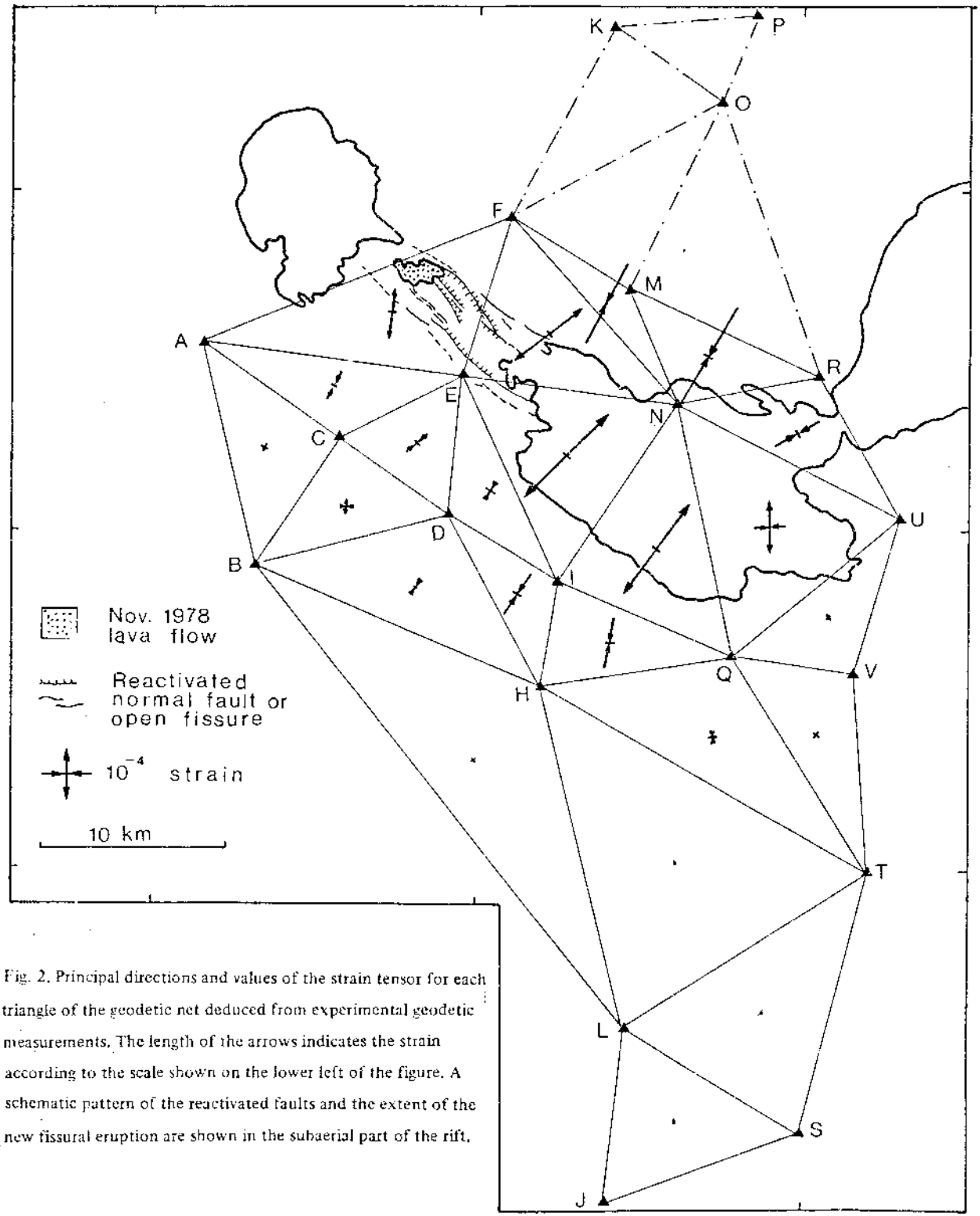

Fig. 2. Principal directions and values of the strain tensor for each triangle of the geodetic net deduced from experimental geodetic measurements. The length of the arrows indicates the strain according to the scale shown on the lower left of the figure. A schematic pattern of the reactivated faults and the extent of the new fissural eruption are shown in the subaerial part of the rift.

brittle threshold (about 1.6×10^{-4} in our case, as we shall see later), the weakest zone, in the inner floor of the rift, breaks and elastic recovery takes place, with faulting, fissuring, and injection of magma (dykes) in the resulting open fissures.

4. A numerical model

In order to test this hypothesis of elasticity, an homogeneous, infinite, two-dimensional horizontal model was assumed, with a 0.27 Poisson's ratio. The model is supposed initially unstressed and in equilibrium. The relative drift of the Arabian and African plates is simulated by an uniaxial strain reaching the threshold value just before the crisis. The crisis itself is then simulated by the opening of some fissures, their locations and sizes being suggested by the pattern of the strain field, and according to the tectonic and seismic data. The minimum number of fissures necessary to fit adequately the data has been found equal to 2 by using trial models.

The model contains ten parameters: the value and orientation of the uniaxial strain field before the crisis (two parameters) and the coordinates of the endpoints of the two fissures (eight parameters) (see Fig. 3).

The strains in our two-dimensional model have been computed using the displacement discontinuity method [10,11]. In this method the exact stress and displacement field in a linearly elastic homogeneous medium are derived, under plane strain condition by means of the Papkovitch functions [12], from the displacement discontinuity existing in a segment with both normal and tangential, non-zero constant values. The solution for an arbitrary boundary geometry is obtained by linear combination of the elementary solutions.

Because we are dealing with strains and not with stresses, the results are independent of the value taken for the Young's modulus.

The computation of trial models by this method leads to results that approach the observed strain field. Nevertheless, since the number of independent observed data ($N = 33$) is larger than the number of model parameters to be determined ($M = 10$), we have decided to use linear inverse methods in order to calculate the best model that fits the data.

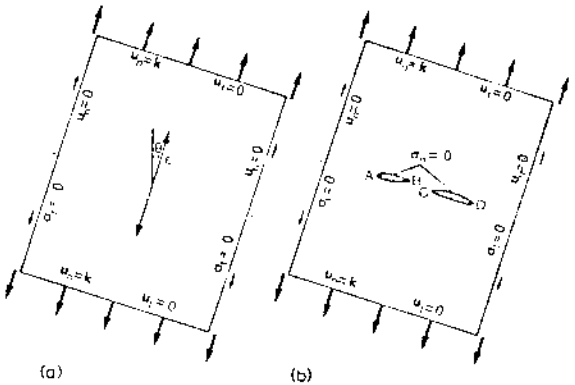

Fig. 3. (a) The model just before the crisis. The first two parameters are the values and orientation of the uniaxial regional strain simulating the relative drift of the Arabian and African plates. (b) The model just after the crisis. Two fissures are allowed to open in the previous field. Strains resulting from this opening are deduced from the difference between stages (a) and (b). The eight coordinates of the four points A, B, C and D, and the two parameters of Fig. 3a, are the parameters of the model. Poisson's ratio is taken equal to 0.27, boundaries are supposed very far from the fissures. u_n, σ_n, u_t, and σ_t are the normal and tangential displacements and stresses imposed as boundary conditions.

5. Results of the inversion

The inversion algorithm used in this study is described in the Appendix. Original data for the inversion are the 33 independent distance changes existing in a geodetic net of 18 points.

Instead of arbitrary choosing these 33 independent data, we take for the inversion routine the 153 relative displacements between all points, in order to provide the same weighting for all points in the inversion.

We have assumed a standard error of 0.05 m for these data. The starting model for the inversion being the last trial model previously obtained. Errors in parameters for this starting model have been assumed to be 0.5×10^{-4} for the regional strain, 10° for its orientation, and 1 km for the coordinates of the endpoints of the two fissures. Partial derivatives are computed numerically by means of the displacement discontinuity method.

The first inversion has given an acceptable result, and no iteration has been needed.

Results of the inversion are listed in Table 2.

TABLE 2

Results of the inversion. The orientation being poorly determined by the data ($D_{22} = 0.93$), no correction has been applied to the starting model for this parameter. The indetermination matrix is defined in the Appendix. Coordinates are given in UTM (grid 38)

Parameter	Indetermination $D_{\alpha\alpha}$	Standard error $\sqrt{\mathrm{Cov}(\Phi_\alpha, \Phi_\alpha)}$	Starting model	Corrections to starting model	Final model
Uniaxial regional strain (elastic-brittle threshold)	0.02	0.09×10^{-4} strain	1.45×10^{-4} strain	0.14×10^{-4} strain	1.59×10^{-4} strain
Orientation of the uniaxial regional strain	0.93	9.6°	45.0°	14.4°	45.0°
Endpoints coordinates					
fissure I	0.09	0.31 km	224.00 km	1.55 km	225.55 km
	0.03	0.17 km	1287.00 km	−2.52 km	1284.48 km
	0.07	0.27 km	230.00 km	−0.69 km	229.31 km
	0.03	0.17 km	1282.00 km	−0.06 km	1281.94 km
fissure II	0.03	0.16 km	233.00 km	1.02 km	234.02 km
	0.07	0.26 km	1279.00 km	0.45 km	1279.45 km
	0.03	0.19 km	240.00 km	1.26 km	241.26 km
	0.03	0.18 km	1275.00 km	0.39 km	1275.39 km

TABLE 3

Comparison between experimental (1) and computed values (2) of the strain tensor components. For each triangle, principal values ($\times 10^{-4}$) are indicated with the direction of the major principal strain

Triangle	(1)	(2)	Triangle	(1)	(2)	Triangle	(1)	(2)
AEF	+1.11	+1.18	EFN	+1.75	+1.78	FMN	+0.05	−0.08
	−0.15	−0.11		−0.18	−0.27		−1.83	−2.03
	7.9°	7.3°		53.0°	50.8°		118.2°	120.3°
MNR	+0.19	+0.19	NRU	+0.19	+0.05	QUV	+0.06	+0.17
	−2.26	−2.29		−1.04	−1.10		−0.07	−0.15
	120.5°	118.7°		150.6°	141.5°		42.9°	44.3°
NQU	+1.08	+1.06	INQ	+2.23	+2.15	EIN	+2.40	+2.32
	−0.57	−0.46		+0.06	+0.03		−0.12	−0.20
	178.2°	179.9°		35.8°	35.4°		44.6°	44.2°
QTV	+0.19	+0.19	BHL	+0.01	+0.06	HLT	+0.02	+0.07
	−0.16	−0.12		−0.12	−0.32		−0.11	−0.11
	47.8°	37.9°		97.1°	124.8°		78.5°	77.4°
LST	+0.04	+0.05	JLS	+0.01	+0.03	HQT	+0.07	+0.22
	−0.01	−0.03		−0.05	−0.05		−0.18	−0.08
	1.7°	52.7°		99.3°	71.9°		78.6°	58.9°
HQI	+0.20	+0.20	DHI	+0.21	+0.15	BDH	+0.04	+0.10
	−0.91	−0.47		−0.92	−0.46		−0.34	−0.22
	100.6°	91.7°		127.2°	133.5°		136.3°	139.6°
BCD	+0.27	+0.11	ABC	+0.10	+0.07	ACE	−0.08	−0.06
	−0.23	−0.14		−0.10	−0.17		−0.69	−0.37
	4.2°	−14.5°		26.2°	−7.0°		117.2°	121.0°
CDE	−0.08	−0.00	DEI	+0.19	+0.11			
	−0.51	−0.37		−0.46	−0.37			
	138.5°	123.1°		122.8°	118.4°			

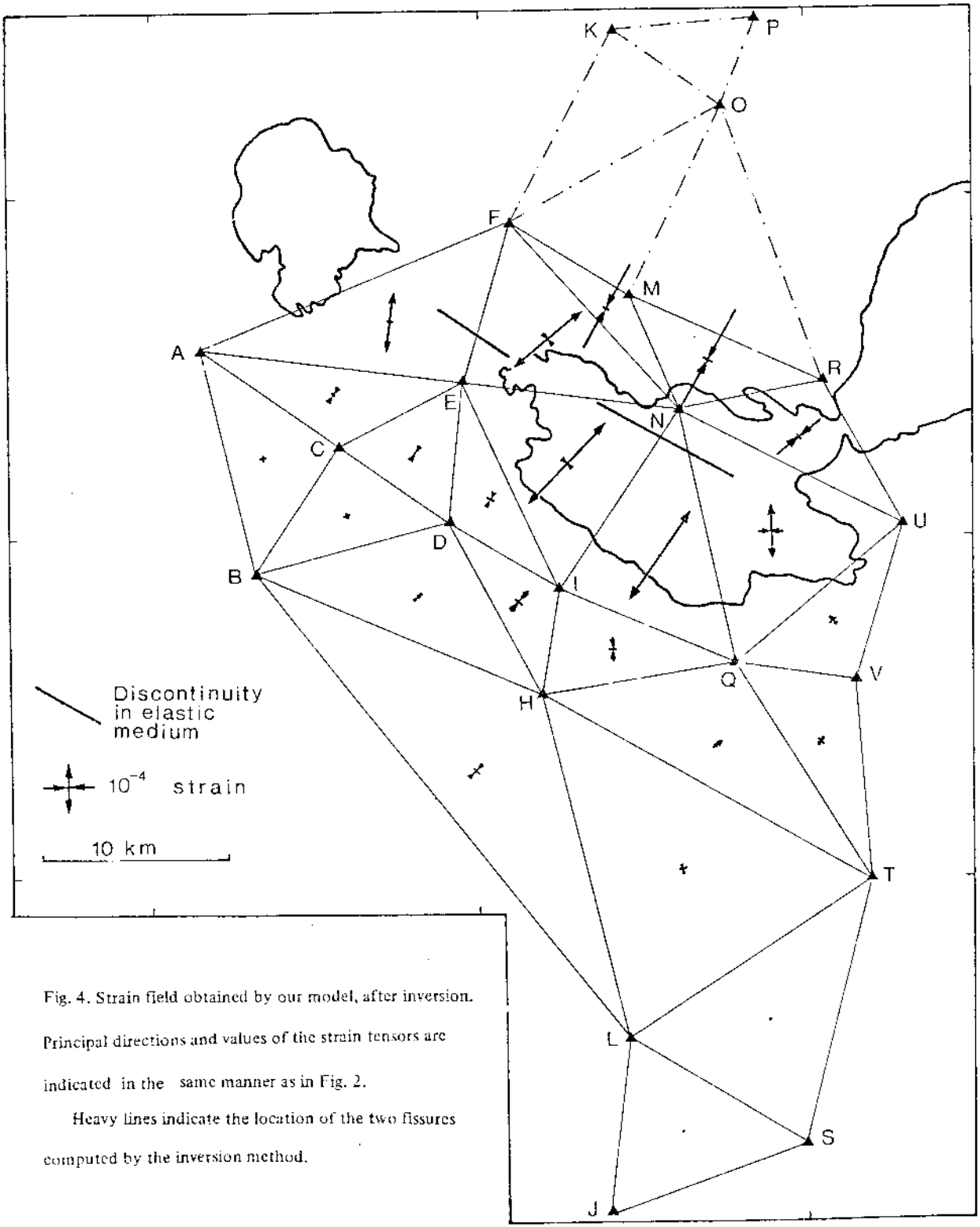

Fig. 4. Strain field obtained by our model, after inversion. Principal directions and values of the strain tensors are indicated in the same manner as in Fig. 2.

Heavy lines indicate the location of the two fissures computed by the inversion method.

6. Discussion

The inverted solution locates one fissure of 4.5 km long which coincides with the axis of the observed subaerial fissure field (Figs. 2 and 4). Its azimuth is 124°N. The second fissure, of 8.1 km long and trending 120°N, is located in the Ghoubbet. Its middle point lies near 11°32.8'N and 42°35.6'E. The value for the elastic-brittle threshold has been found equal to 1.59×10^{-4}. The orientation of the regional strain is poorly determined by the data (see Table 2) and we have kept the value of 45°N from the initial model, which is in agreement with the NE-trending transform faults of the Gulf of Aden's ridge system.

Applying the displacement discontinuity method to this final model, we have computed the strain field shown in Fig. 4. Strain tensors are mean values for each triangle with the previous definition used in Fig. 2.

Results, listed in Table 3, agree surprisingly well with the observed data and the main characteristics and peculiarities of the observed field in Fig. 2 are also found in the model field of Fig. 4.

In Fig. 5 we have plotted the calculated relative displacements versus the measured ones.

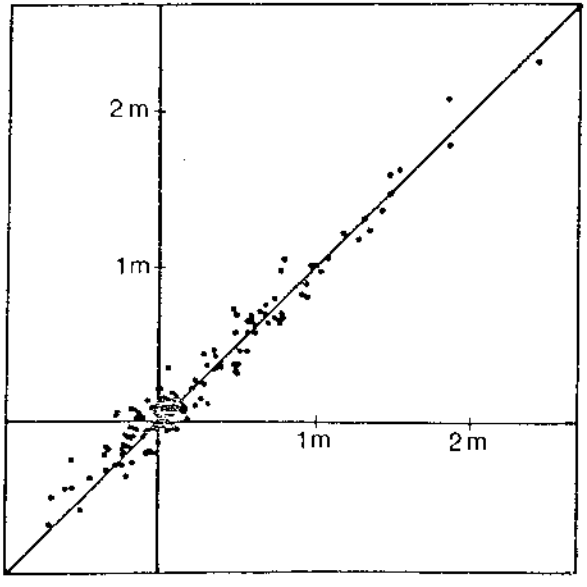

Fig. 5. Computed versus measured distance variations.

The maximum width of the subaerial fissure predicted by the model is found equal to 2.2 m. From our own observations this corresponds to the order of magnitude of the total width of the actual fissuration. In the Ghoubbet, the computed maximum width of the fissure is 3.8 m. A submarine survey of this zone, which is 200 m deep, could reveal important aspects of the recent rifting episode.

Our model, if it can be generalized to other rifting zones, gives information on the mechanical properties of the lithosphere in the accreting plate boundaries [13–15].

Although no geodetic measurements were performed between 1973 and 1978, we have assumed that the whole measured deformation took place during the crisis of November 1978. Two reasons support this assumption: first, the fissure field was extremely fresh when observed in November 1978 [16], secondly, a similar crisis which occurred in Iceland between 1975 and 1978 has shown that horizontal movements are not significant during the years preceding such an event [17,18].

A question remains open: to what extent does visco-plastic deformation take place? Concerning the four points which were surveyed twice in November 1978 and March 1979, relative displacements of a few centimeters have been measured. In any case, such a visco-plastic deformation is an order of magnitude smaller than the elastic deformation in the scale of time considered here. In order to answer this question, geodetic surveys should be regularly conducted in the coming months and years.

8. Conclusion

The good agreement of our model with the geodetic data suggests that an elastic-brittle behaviour of the lithosphere prevailed during the major crisis of November 1978. Our model predicts the location of two fissured zones, one, which was observed, in the subaerial part of the rift, and a submarine one, not yet observed, by 200 m depth. An elastic-brittle strain threshold of 1.6×10^{-4} may represent a typical value beyond which rupture occurs in suboceanic rifting zones, if the Asal-Ghoubbet rift is comparable to other oceanic rifts.

Acknowledgements

We thanks colleagues for helpful discussion, and particularly F.H. Cornet who provided his Fortran IV algorithm for computation of elastic deformation. G. Jobert made useful comments and suggestions. M. Kasser had an essential part in organizat...g the field work and communicated geodetic results prior to publication.

Appendix. Inversion algorithm

Let (ϕ_α) be a vector whose components are the parameters of some initial model, (y_i) be a vector whose components are the values of some measured data, and assume there exists a linear relationship between data and model parameters. The model ϕ being an estimate of the true model and the data having experimental errors, we assume that their covariance matrices $\mathrm{Cov}(\phi)$ and $\mathrm{Cov}(y)$ are known.

We define (Φ_α) and (Y_i) as the best estimators of the true model and the true data, in the least squares sense, i.e. they minimize the χ^2 function:

$$\chi^2 = (Y-y)^t \cdot \mathrm{Cov}^{-1}(y) \cdot (Y-y) + (\Phi-\varphi)^t \cdot \mathrm{Cov}^{-1}(\varphi) \cdot (\Phi-\varphi) \quad \text{(A-1)}$$

with the exact constraint:

$$Y = \mathbf{A} \cdot \Phi \quad \text{(A-2)}$$

where A is the matrix in the linear relation predicted by the theory ("direct problem").

It can be shown [19] that if the covariance matrices have no null nor infinite diagonal elements, i.e. variances, the problem formulated here has always a solution (and a unique one). It is given by:

$$\Phi = [\mathbf{A}^t \cdot \mathrm{Cov}^{-1}(y) \cdot \mathbf{A} + \mathrm{Cov}^{-1}(\varphi)]^{-1} \cdot [\mathbf{A}^t \cdot \mathrm{Cov}^{-1}(y) \cdot y + \mathrm{Cov}^{-1}(\varphi) \cdot \varphi] \quad \text{(A-3)}$$

Calculated parameters (Φ_α) have a covariance matrix that can be defined by:

$$\mathrm{Cov}(\Phi_\alpha, \Phi_\beta) = \sum_{ij} \frac{\partial \Phi_\alpha}{\partial y_i} \frac{\partial \Phi_\beta}{\partial y_j} \cdot \mathrm{Cov}(y_i, y_j) + \sum_{\gamma\delta} \frac{\partial \Phi_\alpha}{\partial \varphi_\gamma} \frac{\partial \Phi_\beta}{\partial \varphi_\delta} \cdot \mathrm{Cov}(\varphi_\gamma, \varphi_\delta) \quad \text{(A-4)}$$

From equation (A-3) it can be shown that this covariance matrix is identical to the first factor in (A-3):

$$\mathrm{Cov}(\Phi) = [\mathbf{A}^t \cdot \mathrm{Cov}^{-1}(y) \cdot \mathbf{A} + \mathrm{Cov}^{-1}(\varphi)]^{-1} \quad \text{(A-5)}$$

Aki and Lee [20] have given a more complicated expression of the covariance matrix for a very similar inverse problem. This is due to the fact that if the initial model ϕ is not explicitly introduced in the definition of the minimizing function χ^2 (equation A-1), then the second term in the right-hand side of equation (A-4) is missing and some simplifications leading to equation (A-5) do not take place.

The "resolution matrix" [21–23] allows to study how parameters are "resolved" by data. We prefer to introduce what we name the "indetermination matrix":

$$D_{\alpha\beta} = \frac{\partial \Phi_\alpha}{\partial \varphi_\beta} \quad \text{(A-6)}$$

From equations (A-3) and (A-6) one obtains:

$$D = \mathrm{Cov}(\Phi) \cdot \mathrm{Cov}^{-1}(\varphi) \quad \text{(A-7)}$$

It can be shown that:

$$0 < D_{\alpha\alpha} \leqslant 1 \quad \text{(A-8)}$$

and it is clear from equation (A-6) that if $D_{\alpha\alpha}$ is close to zero, the parameter Φ_α takes a value independent of the corresponding parameter φ_α of the initial model: the value Φ_α is fixed mainly by the data, i.e. Φ_α is a well "determinate" parameter. If $D_{\alpha\alpha}$ is close to unity, the parameter Φ_α strongly depends on the parameter ϕ_α of the initial model: the parameter Φ_α is "indeterminate".

In fact, the problem we shall treat is not a true linear problem (displacements are not linearly related to our parameters), but because our initial model ϕ is not too far from the final solution Φ, we can, as it is classically done, work in the first-order approximation ("linearized problem"). By expanding in a Taylor's series one obtains:

$$\mathrm{Cov}(\Phi) = [\mathbf{A}^t \cdot \mathrm{Cov}^{-1}(y) \cdot \mathbf{A} + \mathrm{Cov}^{-1}(\varphi)]^{-1} \quad \text{(A-9)}$$

$$D(\Phi) = \mathrm{Cov}(\Phi) \cdot \mathrm{Cov}^{-1}(\varphi) \quad \text{(A-10)}$$

$$\Phi - \varphi = \mathrm{Cov}(\Phi) \cdot \mathbf{A}^t \cdot \mathrm{Cov}^{-1}(y) \cdot [y - f(\varphi)] \quad \text{(A-11)}$$

where $f(\psi)$ are the values of the data predicted from a model ψ (with the non-linear direct problem), and where:

$$\mathbf{A}_{i\alpha} = \left(\frac{\partial f_i(\psi)}{\partial \psi_\alpha} \right)_{\psi = \varphi} \quad \text{(A-12)}$$

are the partial derivatives of the predicted data with respect to the parameters. All other symbols have the same meaning as in equations (A-1) to (A-8).

References

1 H. Tazieff, J. Varet, F. Barberi and G. Giglia, Tectonic significance of the Afar Depression, Nature 235 (1972) 144.

2 L. Stieltjes, Evolution tectonique récente du rift d'Asal (T.F.A.I.), Rev. Géogr. Phys. Geol. Dyn. 15, 4 (1973) 425.

3 C.G.A. Harrison, E. Bonatti and L. Stieltjes, Tectonism of axial valleys in spreading centers: data from the Afar rift, in: Afar Depression of Ethiopia, A. Pilger and A. Rosler, eds. (Stuttgart, 1975) 179–198.

4 H.D. Needham, P. Choukroune, J.L. Cheminée, X. Le Pichon, J. Francheteau and P. Tapponier, The accreting plate boundary: Ardoukoba rift and the oceanic rift valley, Earth Planet. Sci. Lett. 28 (1976) 439.

5 Implantation d'un réseau géodésique pour la mesure directe de l'expansion océanique (Insitut Geographique National, Paris, 1973) 45 pp.

6 M. Kasser, J.C. Lepine and J.C. Ruegg, Mise en évidence de mouvements d'extension sur la dorsale émergée d'Asal-Ghoubbet en République de Djibouti, C.R. Acad. Sci. Paris 288 (1979) 269–272.

7 J.C. Ruegg, J.C. Lépine, A. Tarantola and M. Kasser, Geodetic measurements of Rifting associated with a seismo volcanic crisis in Afar, Geophys. Res. Lett. (in press).

8 J.C. Lepine, J.C. Ruegg and Anis Abdallah, Etude de la crise sismique survenue dans la région de Ghoubbet-Asal (Rep. de Djibouti) en novembre 1978, Proc. 7ème Réun. Annu. Sci. Terre (1979) 293.

9 H.F. Reid, The elastic-rebound theory of earthquakes, Bull. Dep. Geol. Univ. Calif. 6 (1911) 413–444.

10 S.L. Crouch, Solution of plane elasticity problems by the displacement discontinuity method, Int. J. Numerical Meth. Eng. 10 (1976) 301–343.

11 F.H. Cornet, Comparative analysis by the displacement-discontinuity method of two energy criteria of fracture, J. Appl. Mech., Paper 79-APM-25.

12 S.P. Timoshenko and J.N. Goodyear, Theory of Elasticity (McGraw-Hill, New York, N.Y., 1970) 3rd ed., 242 pp.

13 M. Daignières, V. Courtillot, R. Bayer and P. Tapponnier, A model for the evolution of the axial zone of mid-oceanic ridges as suggested by Icelandic tectonics, Earth Planet. Sci. Lett. 26 (1975) 222–232.

14 P. Tapponnier and J. Francheteau, Necking of the lithosphere and the mechanics of slowly accreting plate boundaries, J. Geophys. Res. 83 (1978) 3955–70.

15 V. Courtillot, Opening of the Gulf of Aden and Afar by progressive tearing, Phys. Earth Planet. In. (in the press).

16 B. Robineau, A.Y. Le Dain and P. Tapponnier, Mouvements tectoniques de la crise de novembre 1978 dans le rift d'Asal, Proc., 7ème Reun. Annu. Sci. Terre (1979) 404.

17 A. Björnsson, G. Johnsen, S. Sigurdsson and G. Thorbergsson, Rifting of the plate boundary in North Iceland 1975–1978, J. Geophys. Res. 84 (1978) 3029–3038.

18 J.L. Brander, R.G. Mason and R.W. Calvert, Precise distance measurements in Iceland, Tectonophysics 31 (1976) 193–205.

19 A. Tarantola, F. Albarède, J.C. Lépine, A. Provost, J.C. Ruegg and C. Vincent, A general definition of the linear inverse problem and its application to the determination of the three dimensional velocities of P-waves, (in preparation).

20 K. Aki and W.H.K. Lee, Determination of three dimensional velocity anomalies under a seismic array using first P arrival times from local earthquakes, J. Geophys. Res. 81, 23 (1975).

21 G. Backus and F. Gilbert, The resolving power of gross earth data, Geophys. J. Astron. Soc. 16 (1968) 169–205.

22 G. Backus and F. Gilbert, Uniqueness in the inversion of inaccurate gross earth data, Philos. Trans. R. Soc. London 266 (1970) 123–192.

23 D.D. Jackson, The use of a priori data to resolve non-uniqueness in linear inversion, Geophys. J.R. Astron. Soc. 57 (1979) 137–157.